Research article

Fetal ECG signal processing and identification of hypoxic pregnancy conditions in-utero

Tetiana Biloborodova[1], Lukasz Scislo[2], Inna Skarga-Bandurova[3], Anatoliy Sachenko[4,5,*], Agnieszka Molga[4], Oksana Povoroznyuk[6] and Yelyzaveta Yevsieieva[7]

[1] Department of Computer Science and Engineering, Volodymyr Dahl East Ukrainian National University, 43 Donetska Street, Severodonetsk 93400, Ukraine

[2] Faculty of Electrical and Computer Engineering, Cracow University of Technology, Warszawska 24 Street, Cracow 31155, Poland

[3] School of Engineering, Computing and Mathematics, Oxford Brookes University, Wheatley Campus, Oxford, OX33 1HX, UK

[4] Department of Informatics, Kazimierz Pulaski University of Technology and Humanities in Radom, Radom 26600, Poland

[5] Research Institute for Intelligent Computer Systems, West Ukrainian National University, Ternopil 46009, Ukraine

[6] Department of Computer Engineering and Programming, National Technical University "Kharkiv Polytechnic Institute," 2 Kyrpychova Street, Kharkiv 61002, Ukraine

[7] School of Medicine, V. N. Karazin Kharkiv National University, 4 Svobody Square, Kharkiv 61002, Ukraine

* **Correspondence:** Email: as@wunu.edu.ua.

Abstract: The fetal heart rate (*f*HR) variability and fetal electrocardiogram (*f*ECG) are considered the most important sources of information about fetal wellbeing. Non-invasive fetal monitoring and analysis of *f*ECG are paramount for clinical trials. They enable examining the fetal health status and detecting the heart rate changes associated with insufficient oxygenation to cut the likelihood of hypoxic fetal injury. Despite the fact that significant advances have been achieved in electrocardiography and adult ECG signal processing, the analysis of *f*ECG is still in its infancy. Due to accurate fetal morphology extraction techniques have not been properly developed, many areas require particular attention on the way of fully understanding the changes in variability in the fetus and implementation of the non-invasive techniques suitable for remote home care which is increasingly in demand for high-risk pregnancy monitoring. In this paper, we introduce an integrated approach for

ƒECG signal extraction and processing based on various methods for fetal welfare investigation and hypoxia risk estimation. To the best of our knowledge, this is the first attempt to introduce the auto-generated risk scoring in ƒECG to achieve early warning on fetus' safety and provide the physician with additional information about the possible fetal complications. The proposed method includes the following stages: ƒECG extraction, ƒHR and fetal heart rate variability (ƒHRV) calculation, hypoxia index (HI) evaluation and risk estimation. The extracted signals were examined by assessing Signal to Noise Ratio (SNR) and mean square error (MSE) values. The results obtained demonstrated great potential, but more profound research and validation, as well as a consistent clinical study, are needed before implementation into the hospital and at-home monitoring.

1. Introduction

Fetal heart activity tracking and wellbeing investigation is an essential part of prenatal care. Clinical fetal monitoring based on both antepartum ƒHR and ƒECG shows that most of the cardiac defects, as well as oxygen deprivation, have some appearance in the ƒECG morphology. In this sense, electrocardiography could be seen as one of the most important reference sources about fetal status during pregnancy and at labour with a high predictive value. This information can be exploited to diagnose fetal hypoxia and indicate changes in fetal heart patterns. Fetal heart monitoring serves the purpose of detecting signs of life in utero, including abnormal ƒHR or patterns, which may indicate oxygen deficiency or other pathological processes at their early stage to perform the appropriate intervention and prevent intrauterine fetal neurological damage and mortality. Besides other metabolic changes, fetal response to oxygen deprivation includes decreased heart rate, cessation of gross body movements and a reduction in oxygen consumption [1,2]. These changes enable to use of ƒHR monitoring as a potentially valuable approach for assessing hypoxaemic fetus and their oxygenation status in real-time. In addition, accurate identification of fetuses with sufficient heart rate and oxygenation can prevent unnecessary intervention; reduce the fetal morbidity and number of operative deliveries [3].

Although the ƒHR changes markedly during uninterrupted hypoxia, fetal deprivation or non-reassuring fetal status can be observed only indirectly. To date, the majority of ƒECG studies on long-term electronic fetal monitoring are based on data acquired on a clinical basis which requires costly equipment, extensive training, a high level of technical skill, and is subject to high variability in data interpretation. To overcome these challenges, significant efforts are being made for both remote solutions for home ƒHR monitoring and signal processing technique. While the current standards of fetal monitoring do not support remote or at-home monitoring and require a high skilled physician to interpret results, research community and medical systems developers tend to capacity building and development of non-invasive, portable devices feasible to telemedical home care and long-term monitoring of ƒHR and ƒECG [4–6]. This is particularly relevant for developing countries and rural areas where access to prenatal care can be challenging due to different reasons, including physician scarcity, unavailability of equipment for accurate record keeping and peculiarities of rural geography. Moreover, remote, outpatient ƒHR monitoring provides the means to collect and analyze large ECG

data, enabling pregnant women to receive timely prenatal and antenatal care, which is crucial in high-risk pregnancies.

A new generation of perinatal care instruments offers the capability to deliver an undistorted *f*ECG output from electrodes placed on the maternal abdomen, perform advanced morphological *f*ECG signal extraction and analysis, and send raw and proceeded data directly to the physician. The idea is to develop a tool being intrinsically ambulatory, could also to perform signal recording and processing in the home environment on a long-term basis [7] and offering the capability to carry out advanced morphological *f*ECG signal analysis [8]. Improvement of technology for *f*HR monitoring is promising; however, it has not yet reached a sufficient level of accuracy to be approved for commercial devices [9]. A limitation of this approach is that it utilizes a just noticeable, very low signal to noise ratio (SNR). Most notably, this is because the *f*ECG signal is produced by the fetal heart that is a relatively small source compared to the mother's body. In particular, the size of the maternal electrocardiogram (*m*ECG) found in the abdominal cavity is approximately 2–10 times the size of the *f*ECG [10], which also makes it difficult to extract the *f*ECG. Moreover, received abdominal signal includes not only *m*ECG and weak signals of *f*ECG but also other signals as maternal respiration, the electrohysterogram (EHG), the power line interference, and other noise coming mainly from maternal muscle activity. Thus, the suppression of *m*ECG while preserving the fetal QRS complex is the most important stage in the *f*ECG extraction from the maternal abdominal signal [11]. Further development and evaluation of these technologies remain a global priority.

The present study is a continuation of the previous work [12] aimed at discovering interesting associations in gestation course data and finding risk factors in pregnancy-related to fetal hypoxia. Our current goal is to automate the in-utero fetal hypoxia risk factors detection to achieve early warning on fetus' safety and provide the physician with additional information about the potential threat, if any. We investigate the possibilities of *m*ECG elimination and *f*ECG extraction from signal recorded non-invasively on the mother's abdomen and assess the feasibility of the *f*ECG morphological evaluation to be included in the automatic screening tool for identifying fetuses at high risk of hypoxia. To be adopted with this process, we propose a novel methodology for automatic *f*ECG signal processing and tune it into a fetal hypoxia risk-scoring tool. To our knowledge, this is the first trial to introduce auto-generated risk scoring in *f*ECG. It is assumed that risk evaluation allows early warning on fetus' non-reassuring fetal status and provides the physician with additional information about the possible fetal complications.

2. State of the art

Several surveys and systematic reviews of *m*ECG elimination and *f*ECG detection were found in the literature. In [13], the most common techniques developed over the last four decades with discussion both their advantages and shortcomings are given. Another review [14] is devoted to *f*ECG signal processing and *m*ECG cancelling methods based on the power line interference component (PLI). In [15], the system for indirect *f*ECG was proposed and evaluated with direct *f*ECG, which currently is the gold standard of *f*ECG.

A comparative analysis of single-channel *f*ECG extraction methods is given in [16]. In the vast majority of cases, *f*ECG is obtained from multichannel devices by evaluating independent sources of fetal heart bioelectrical activity [17]. While extracting unobservable signals, the sources are assumed to be statistically uncorrelated to each other and the known mixture of these signals [18]. In many

practical applications, the multichannel ƒECG extraction is based on Blind Source Separation (BSS) and its variations as BSS with Reference (BSSR) [19] and others. The study on this topic based on a solid theoretical approach known as Independent Component Analysis (ICA) [20] which requires the use of Higher-Order Statistics (HOS). However, for some cases as Gaussian sources, HOS methods do not allow to perform the separation. An alternative approach for source separation is second-order statistics (SOS). SOS-based methods include Singular Value Decomposition (SVD) [21], Principal Component Analysis (PCA) [22, 23], Periodic Component Analysis (πCA) [24], etc. Besides, many other methods have been applied for the same purpose, such as Extended Barros's extraction algorithm and Zhang algorithm (ZA) [25], polynomial eigenvalue decomposition (PEVD) [26], generalized eigenvalue decomposition (GEVD) [27], fuzzy clustering c-means (FCM) [28], Compressed Perception (CS), parental suppression method (MCSM), Hilbert Huang Transform (HHT) [29], and others. Figure 1 shows a comparison of the most popular multichannel methods for ƒECG signal separation. Following the idea discussed in [30], ten approaches were compared according to their overall performance, SNR improvement level, computational cost, and implementation complexity. We used blue lines for real-time approaches and red lines for non-real-time approaches.
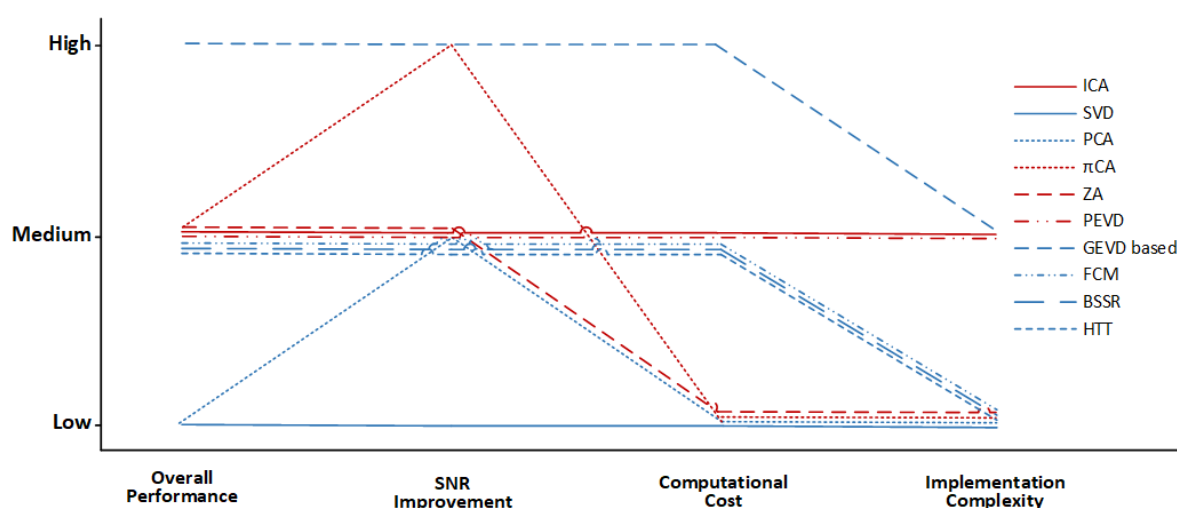

Figure 1. The landscape of comparison for the multichannel methods used for ƒECG extraction.

The ICA can be seen as a baseline technique since this is the most popular non-adaptive method for ƒECG extraction and has the average characteristics across the board. There are many modifications of the ICA technique discussed in the literature, including the Fast ICA algorithm (FastICA) [31], Joint Approximate Diagonalization of Eigen matrices algorithm (JADE) [32]. In [33], three-lead abdominal ECG (aECG) signals are collected and sent to the smartphone application, where the signal is processed using the FastICA algorithm to extract the signal components. The sample's entropy is used to determine the ƒECG signal and calculate the ƒHR. In [34], the Space-Time ICA (ST-ICA) was implemented by combining the delays with FastICA. The preliminary results indicate that the temporal dynamics and the spatial information used by ST-FastICA enable a robust separation of ECGs in low-dimensional recordings where the traditional implementation of FastICA is more likely to fail. The SVD is a spatial filtering approach that seeks a linear decomposition of a data matrix, which acts as a spatial filter and efficiently removes electrocardiographic artefacts [17]. PCA is a method that is often

used to reduce the dimensionality of large data sets. PCA might also be applicable to find a linear combination of vectors and separating mixed signals from statistically independent sources. Transforming the data into a new orthogonal coordinate system enables us to find the most significant vectors, and this operation increase interpretability while minimizing the loss of information [35]. The polynomial matrix eigenvalue decomposition (PMED) method is an extension of EVD in the case of the para-Hermitian matrix. It represents polynomially (or convolutively) mixed signals in the diagonal matrix form. This transformation provides both improved signal and noise identification and strong decorrelation.

The subspace decomposition enables signal separation and estimation of the *f*ECG signal. PMED is a blind approach that does not require a priori knowledge of the source signals or the mixing matrix; instead, it utilizes the space-time covariance matrix's information carried by the observed sensor signals. Assuming that source signals to be statistically independent, the *m*ECG amplitude can be compared to *f*ECG to separate from *a*ECG [26]. PMED does not require *m*ECG as a reference and shows relatively low sensitivity to sensor placement.

An analysis of *m*ECG suppression techniques shows that more accurate results are obtained mainly with hybrid non-adaptive methods [36,37], ICA & PF [38]. The methods' performance highly depends on the tasks for which they are applied (filtering, correlation, transformation, separation, etc.), which also explains the advantage of hybrid methods. In many cases, non-adaptive methods are used for preprocessing, and further analysis is performed with adaptive algorithms. Applying non-adaptive techniques enables partially separate source components and facilitate retrieval for an adaptive system. By this reasoning, we use a hybrid approach for *f*ECG extraction and fetal R-peaks detection, which incorporates the ECG signal's periodic nature and shows the accuracy of *f*ECG extraction sufficient for its analysis. At the stage of the *f*ECG extraction, the following techniques have been applied: PCA to determine the correlation between layering, JADE for blind signal separation, GEVD and πCA for separation of the *m*ECG and *f*ECG.

3. Materials and methods

Proposed *f*ECG signal processing and hypoxia risk estimation pipeline comprises the following stages: 1) *f*ECG extraction and separation, 2) *f*HR and *f*HR variability (*f*HRV) calculation, 3) hypoxia index (HI) evaluation and risk estimation. We detail the basic mathematical concepts and procedures step by step below.

3.1. Fetal ECG extraction and separation

The data model of signals received from the maternal abdominal surface can be represented as follows [39]

$$x(t) = H_m s_m(t) + H_f s_f(t) + H_v v(t) + n(t), \qquad (1)$$

where $x(t) \in \mathbb{R}^N$ denotes the *N*-channel measurements from the surface of the maternal abdomen and thoracic, $s_m(t) \in \mathbb{R}^M$ describes the *m*ECG entry, $s_f(t) \in \mathbb{R}^L$ are the *f*ECG components, $v(t) \in \mathbb{R}^K$ and $n(t) \in \mathbb{R}^N$ denotes the correlated (low-rank) noise and uncorrelated (full-rank) noise respectively; $H_m \in \mathbb{R}^{N \times M}$ and $H_f \in \mathbb{R}^{N \times L}$ matrices describe the signals received from a set of electrodes placed on the surface of the maternal body. Eq (1) in a compact form:

$$x(t) = [H_m \; H_f \; H_v] \begin{bmatrix} s_m(t) \\ s_f(t) \\ s_v(t) \end{bmatrix} + n(t) = Hs(t) + n(t), \tag{2}$$

here matrix $H \in \mathbb{R}^{N \times (M \times L \times K)}$ is a general mixing matrix through the sources and $s(t) \in \mathbb{R}^{M \times L \times K}$ represents all sources and structural noise jointly. When the general mixing matrix H is non-singular and the number of monitored channels N is equal to or greater than the effective number of M, L, K sources ($N \geq M + L + K$), the observed mixture can be treated as defined or redefined. Thus, $s_m(t), s_f(t)$ and $v(t)$ are considered as groups of mutually independent sources with some internal correlations.

The *f*ECG extraction procedure is summarized in Figure 2, with key elements described in detail below. In a generic way, the procedure comprises of six stages: 1) signal preprocessing, 2) *m*ECG R-peak detection, 3) sources separation, 4) *m*ECG cancellation, 5) *f*ECG R-peak detection, 6) *f*HR analysis for detection of fetal hypoxia. At the first stage, six maternal ECG signals (five abdominal and one thoracic) are preprocessed. The key operations include removing the baseline wander and cancelling higher frequency content with a second-order zero-phase low pass filter. On stage two, PCA decorrelation is applied. The *m*ECG R-peak detection occurs on each pre-filtered channel, including PCA-transformed one.
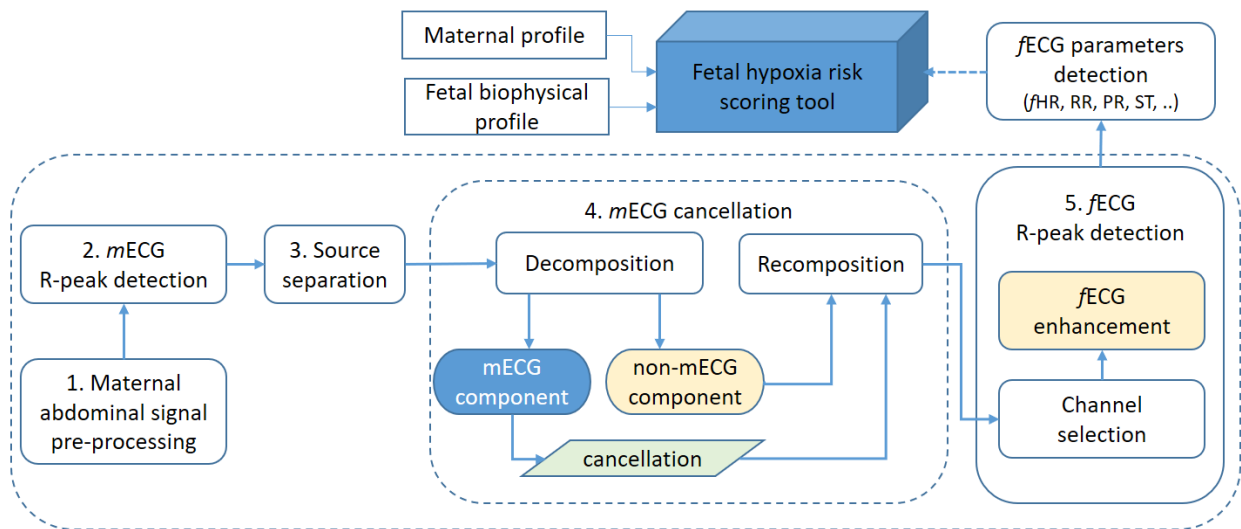

Figure 2. Block diagram of the *f*ECG extraction procedure built into fetal hypoxia risk scoring tool.

As a result, one of the *m*ECG R-peak channels is selected as being the reference component. The third stage runs the source separation algorithm on the *a*ECG data with the purpose of extract the *f*ECG. On stage four, the *m*ECG channels are cancelled using generalized eigenvalue decomposition and periodic component analysis. Stage five assumes *f*ECG R-peak detection is performed based on the residuals containing the *f*ECG through the *f*ECG enhancing. Finally, a channel for *f*ECG R-peak detection is selected. Finally, extracted *f*ECG R-peak and corresponding *f*HR are scored for detection of fetal hypoxia. Below all the steps are presented and explained in more detail.

3.1.1. Signal preprocessing

As it was mentioned above, readings obtained from the maternal surface include three types of data, 1) mix of low-amplitude *f*ECG signal together with *m*ECG signal, 2) high-amplitude baseline wander and 3) noise. The preprocessing stage involves the techniques for eliminating low frequency (below 0.05 Hz) baseline wander and removing high-frequency (above 50 Hz) noise from each channel. For this purpose, the second-order zero-phase low pass filter is used.

3.1.2. The *m*ECG R-peak detection

The *m*ECG R-peak is detectable from an independent maternal thoracic lead. The principal component analysis helps to obtain the maternal component for R-peak detection. To increase the *m*ECG R-peak contribution on the principal components, the *m*ECG R-peak detection is executed per both pre-filtered channels and channel after PCA transformation. As a result, one of the *m*ECG R-peak channels is selected as being the reference channel.

3.1.3. Source separation

The source separation is carried out on the *a*ECG to extract the *f*ECG. With respect to the data model (1), this step assumes a specific separation of *f*ECG from the structured noise $v(t)$. From our previous analysis, BSS can be used to take advantage of the inter-channel spatial correlation of *f*ECG sources, slightly improving the quality of *f*ECG before detecting R-peaks. Namely, the JADE algorithm [40] is used. The number of extracted components is the same as the number of maternal channels recorded from the surface of the abdomen and chest of a pregnant woman.

It should also be mentioned that due to the peculiarities of the implementation of a blind source separation algorithm, the order of the putative sources (in our case *f*ECG) could not be guaranteed. This requires additional visual inspection of each *f*ECG channel after the JADE has been applied.

3.1.4. The *m*ECG cancellation

Whereas the *m*ECG is considered as the main source of interference in *f*ECG, iterative subspace decomposition is applied to eliminate maternal components from the recordings. As a basis for our method, we used the approach proposed in [41] and modified it as follows.

First, we run GEVD to address the challenge with source separation. The GEVD of a pair of matrices (A, B) generalizes the EVD of a single matrix and produces the new matrices W and D in such way that

$$W^\mathsf{T}AW = D, \quad W^\mathsf{T}BW = I, \tag{3}$$

where $A, B, D, W, I \in \mathbb{R}^{N \times N}$ and A, B are initial symmetric matrices to be diagonalized, D denotes the generalized diagonal matrix of eigenvalues correspond to the generalized eigenvalue W with a set of real eigenvalues sorted in ascending order along its diagonal, and I is the identity matrix.

Using GEVD, the pair of matrices are computed over the entire data set. The efficiency of linear decomposition with GEVD vary with the utilization of preliminary signal and noise subspace information collected in matrix pairs A and B.

Next, a linear source separation on πCA [42] was applied to the new matrix pairs. The periodic component analysis utilizes the concept of cardiac phase to sequentially change the ECG rhythm on a controlled rhythm. The algorithm calculates the timespan τt for which the ECG signal $x(t)$ maximally correlate with $x(t + \tau t)$. The πCA is purely compatible with the pseudo-periodic structure underlying the maternal and fetal signals and can be evaluated using the cost function as follows

$$J(W) = \frac{W^\mathsf{T} E_t \{x(t)x(t - \tau_t)^\mathsf{T}\}W}{W^\mathsf{T} E_t \{x(t)x(t)^\mathsf{T}\}W} = \frac{W^\mathsf{T} C_\tau W}{W^\mathsf{T} C_x W}, \tag{4}$$

here τ_t denotes the interested timespan for the corresponding ECG, C_τ refers to the lagged covariance matrix calculated over the timespan τ_t and W is a matrix resulting from GEVD of diagonalized matrices C_x and C_τ.

The method reapplies a linear decomposition sequence to autonomously separate the *m*ECG and *f*ECG subsets, followed by noise removal for suppressing the *m*ECG components, and finally, the background projection of the disabled elements into the input data space. This is an iterative procedure repeatedly carrying out a process until most of the maternal components removed from the *f*ECG. In this regard, the preprocessing stage where simple R-peak detection is performed enables to detect the location of the maternal R-peaks. This information is passed to the *m*ECG cancellation module, where fine-grained separation and sorting of the *m*ECG and *f*ECG components formed with respect to the degree of similarity across their periodic properties and the frequency of the *m*ECG signal.

3.1.5. The *f*ECG R-peak detection

At this step, *f*ECG is enhanced using the FastICA algorithm as an additional filter and a channel for *f*ECG R-peak detection is selected. The *f*ECG R-peaks detection carried out via a dedicated *f*ECG channel using the following procedure. The selected *f*ECG component is run through a matched filter with a narrow *f*ECG R-peak amplitude for maximizing its impulse response. The amplitude is specified further to visual inspection of the output. Then the results are squared and time-averaged through a moving average filter. The resulting local peaks can be thought-out as the fetal R-peaks.

3.2. Fetal ECG parameters detection

The *f*HR and *f*HRV are the primary sources of information about fetal well-being. Instantaneous *f*HR in beats per minute (bpm) is calculated for each cardiac cycle T (in milliseconds) as stated by Eq (5) [43].

$$fHR = \frac{60000}{T}. \tag{5}$$

Following recommendations of the heart variability standard [44], time and frequency analysis of the *f*HR is calculated on 5-minute segment blocks.

For the *f*HR values $s[n]$ ($n = 1, ..., N$), also denoted in a vector form as $\bar{s}$, the *f*HR baseline variability (*f*HRV) is considered as the sign of severe fetal brain damage [45]. The *f*HRV is represented in the time domain as follows

$$\overline{fHRV} = \bar{s} = \frac{1}{N} \sum_{n=1}^{N} s[n]. \tag{6}$$

3.3. Hypoxia index (HI) evaluation and risk estimation

Considering the fact that intrapartum *f*ECG could be used as a screening method for detecting hypoxia [46], it would be safe to assume that hypoxia risk estimation is achieved through the hypoxia index (*HI*) proposed in [47], at least for the labor stage. The threshold *HI* for a set of *f*HR values s[n] is the sum of all deceleration periods (min) divided by the lowest *f*HR (bpm) in the decelerations, multiplied by 100. The resulting value indicates the intensity of hypoxia in the intrapartum fetal heart rate monitoring.

Denoting one period of deceleration of *f*HR *Tdec*, and the lowest value of *f*HR as *f*HRmin_dec, the threshold hypoxia index *HI* can be expressed as follows

$$Hi = \frac{\sum_{n=1}^{N} T_{dec}}{fHR_{\min\_dec}} \cdot 100. \tag{7}$$

The fetal hypoxia risk assessment is performed in accordance with [48], where the value of the $Hi = 25$ is a threshold level, for values greater than 25, the risk of fetal hypoxia shall be considered as high. With a calculated hypoxia index of $Hi \leq 24$, the risk of fetal hypoxia is considered low.

Additional information for detecting fetal distress can be obtained by a more profound analysis of the morphology of the *f*ECG signal, e.g., the ratio between the amplitude of the fetal QRS complex and that of the T wave, ST-segment changes, etc., to be included in the risk scoring tool.

4. Experiment and results

We tested the implementation of the first stage of the *f*ECG extraction for automatic processing and analysis of ECG and risk assessment of hypoxia. The experiment was performed using the Open-source electrophysiological instrument set (OSET) tools [49]. As a result, the *f*ECG was isolated, and R-peaks were determined.

4.1. Data description

For this experiment, the dataset [50] from PhysioNet [51] were used. Non-invasive fetal ECG signals were collected using routine abdominal electrocardiography. The *f*ECG data came from the automated Cardiolab Babycard fetal monitor. The data consist of records in which fetal arrhythmias are diagnosed by echocardiography and equal control records in which normal rhythm is diagnosed. Records are annotated as follows: ARR - fetal arrhythmia, NR - normal fetal rhythm. The experiment used 10-second fragments of records NR_02 and ARR_01.

Each record is with a record of four or five abdominal channels-abdominal ECG (*a*ECG): Abdomens_1–5 and one thoracic lead, which corresponds to the selected ECG of the mother-maternal ECG (*m*ECG). The experiment performed 10-second fragments of records ARR_01 and NR_02. The

sampling frequency of signals is 1000 Hz. The fragments of records ARR_01 and NR_02 are as follows (see Figures 3 and 4). In Figures 3 and 4, the upper signal corresponds to the thoracic lead, i.e., the *m*ECG, the five lower signals correspond to the *a*ECG.
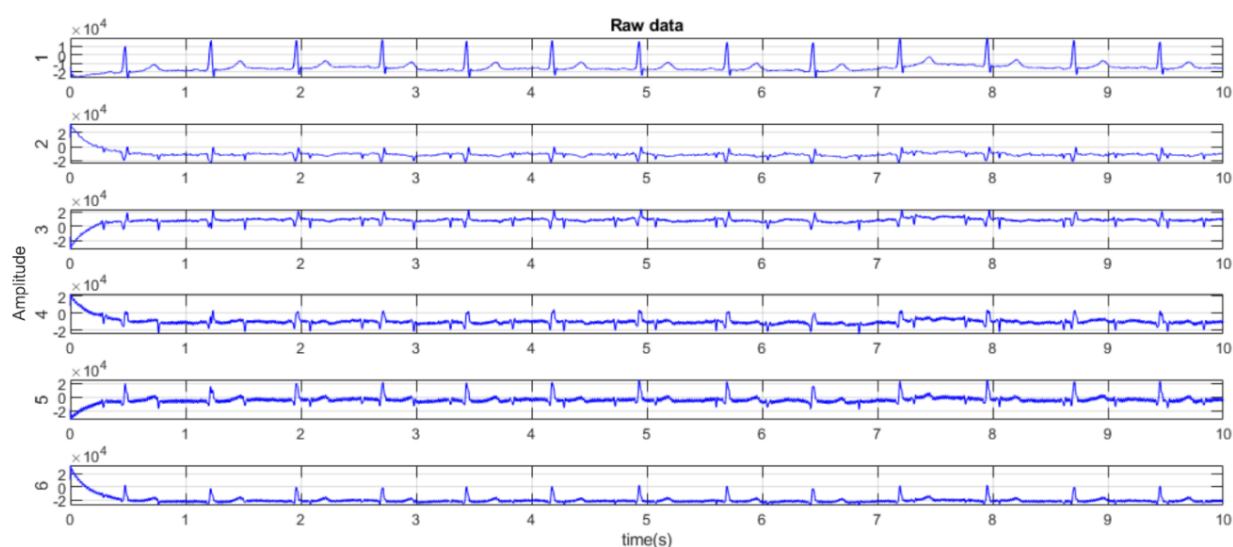

Figure 3. The raw data of ARR_01.

Raw signals from abdominal channels contain not only the *fECG* but also primarily the *mECG* and various types of noise (e.g., maternal muscles activity or artifacts resulting from fetal movements).
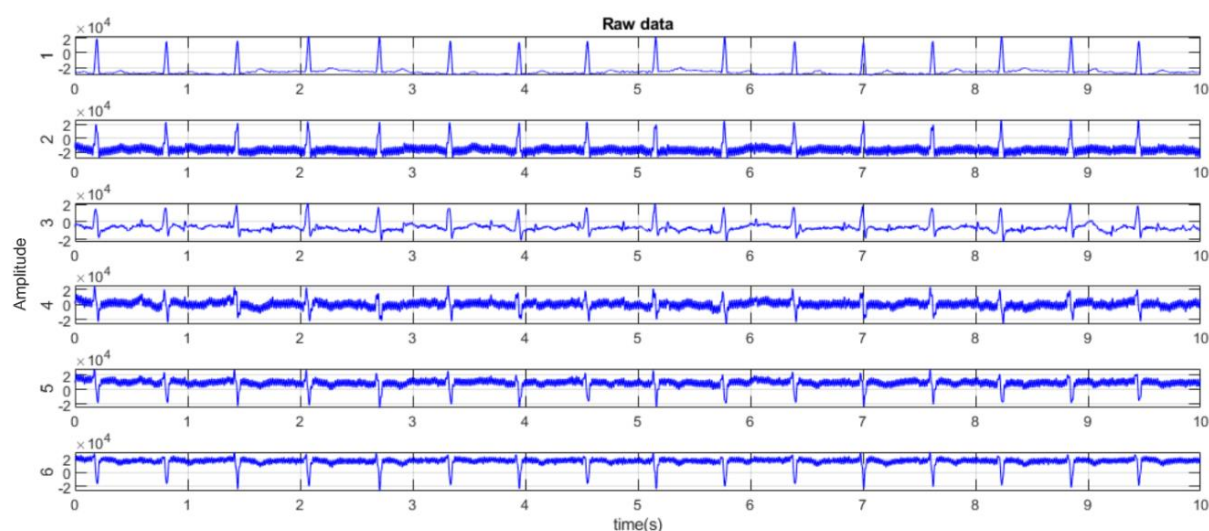

Figure 4. The raw data of NR_02.

From Figures 3 and 4, the initial raw data under identical conditions, however, are visually different. This may be due to even the slightest difference in the location of the electrodes, the position of the fetus, the different ADC noises and many other factors that affect the ECG properties of the fetus discussed above.

4.2. fECG extraction

Firstly, the preprocessing step was conducted by means of a second-order zero-phase lowpass filter with the parameters described above. The filter removes data from the baseline wander and cuts-off high-frequency values equal to 50 and 60 Hz. The data ARR_01 and NR_02 after the preprocessing are presented in Figures 5 and 6. It can be observed that, unlike the raw data, there is no baseline wander in the processed.
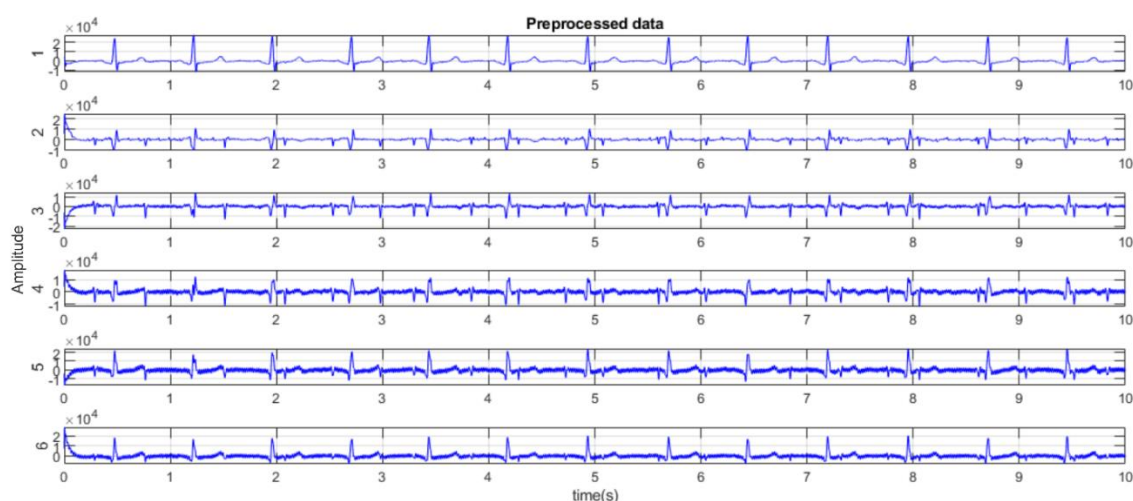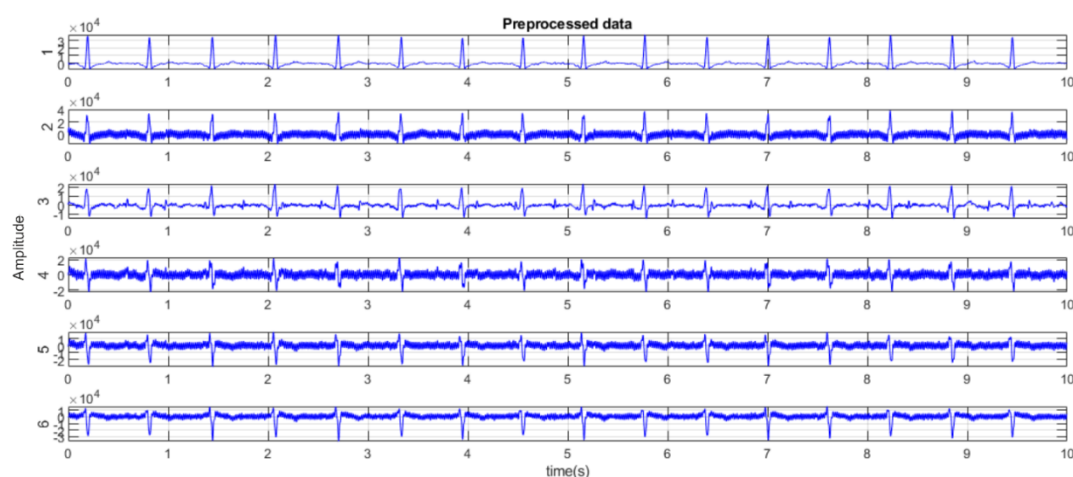

Figure 5. Preprocessed data ARR_01.

Figure 6. Preprocessed data NR_02.

The preprocessing parameters are defined in such a way as to remove the most of noise while preserving the elements of the fetal and maternal QRS complexes. Signal processing with a low pass filter enables filtering out the dc potentials that trigger the baseline wander.

At the next step, the principal component analysis (PCA) was applied for maternal R-peak detection. In general, PCA enables to reduce the data dimensionality while preserving their informative

value. With fECG extraction, isolating the main components of the fetal ECG signal is complicated by the fact that even after filtering, the data contains noises that, along with the fetal and maternal ECG signals, will affect the dimension of the extracted components. Data of ARR_01 and NR_02 after the principal component analysis are presented as follow (see Figures 7 and 8).
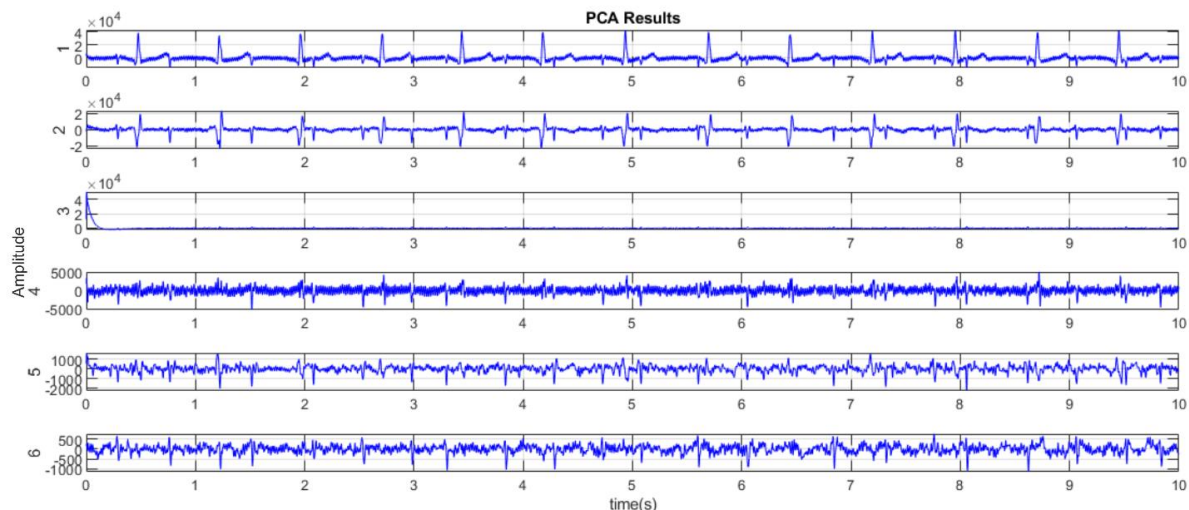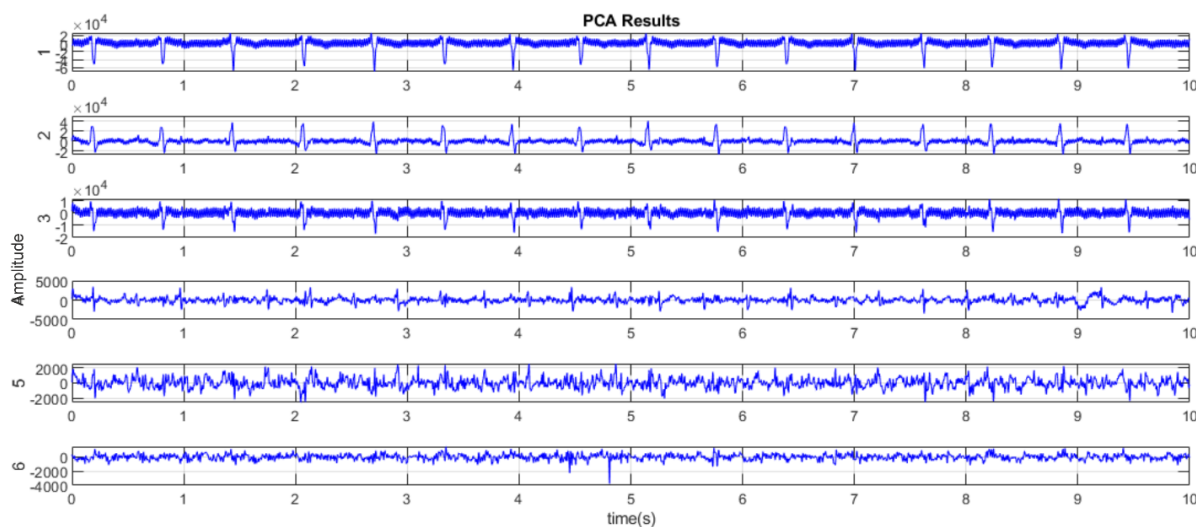

Figure 7. The results of the PCA of ARR_01.

Figure 8. The results of the PCA of NR_02.

In this matter, PCA is, in a way, signal preprocessing before extracting independent components using JADE. Following the overall procedure, the *m*ECG was used for blind source separation using the JADE algorithm. The results of source separation of ARR_01 and NR_02 are presented in Figures 9 and 10.
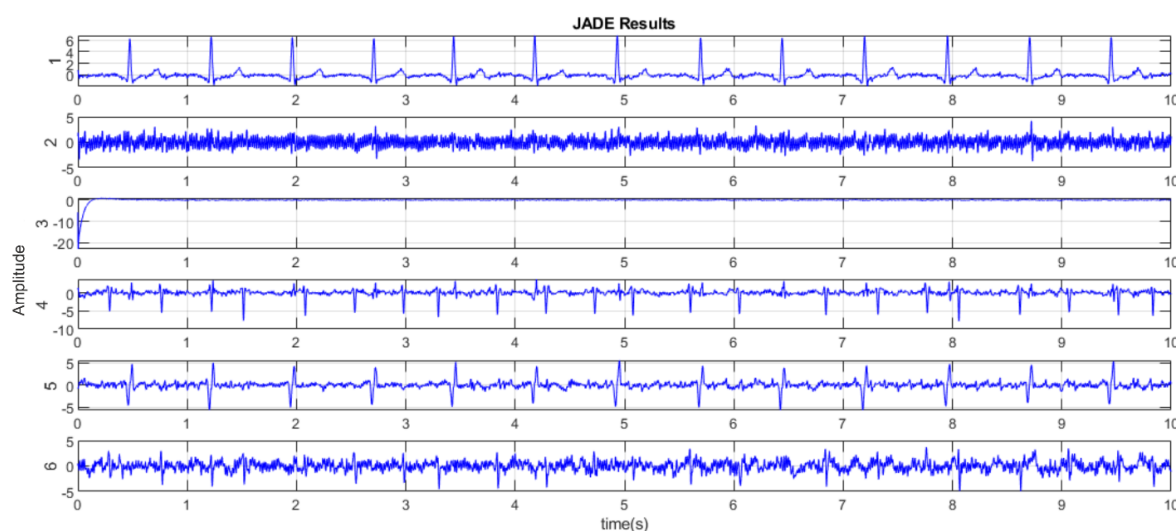
Figure 9. The results of source separation of ARR_01.

For ARR_01, 2 out of 6 extracted components clearly correspond to the maternal ECG (1 and 5), two components correspond to the fetal heart (4, 6), and two components comprise the noise (2, 3). Based on the results of source separation, channel 4 was selected for ƒECG extraction for ARR_01, and channel 1 was selected for more accurate *m*ECG extraction.
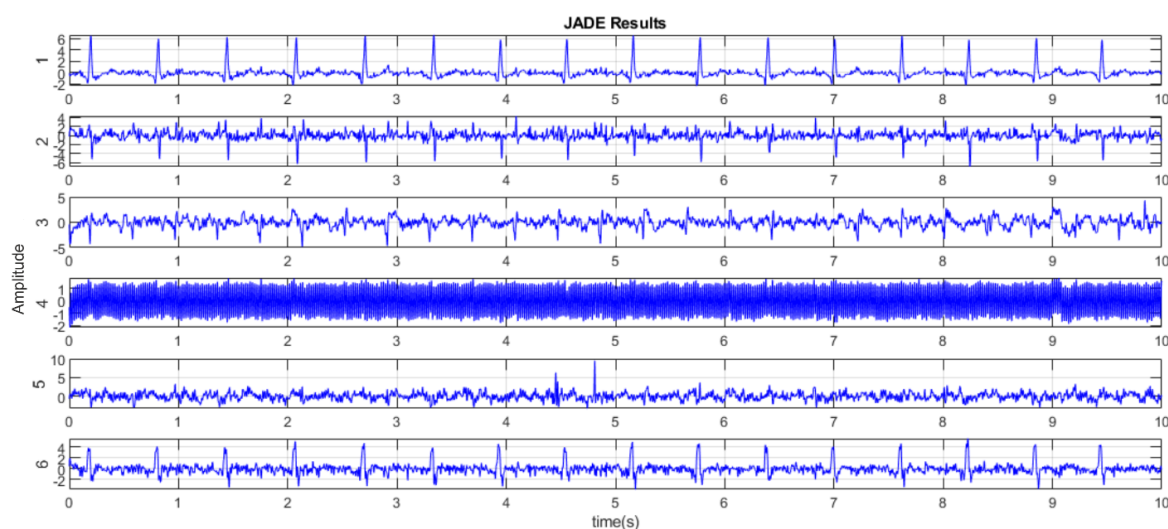

Figure 10. The results of source separation of NR_02.

For NR_02, 2 out of 6 extracted components clearly correspond to the maternal ECG (1 and 6), two components correspond to the fetal heart (2, 3), and two components comprise to the noise (4, 5). Based on source separation results, channel 2 was selected for ƒECG extraction and channel 1 for more accurate *m*ECG extraction.

After *m*ECG cancellation, signals be subject to the GEVD and periodic component analysis for ƒECGs extraction. In ARR_01, the R-peaks of the selected independent fetal component (4) are used to calculate the fetal ECG period. The results of the periodic component analysis for ARR_01 are

shown in Figure 11. As seen, the first component (corresponding to the largest eigenvalue) bears the most significant similarity to the fetal ECG, while as the eigenvalues decrease (from the first to the last component), the signals become less similar to the *f*ECG.
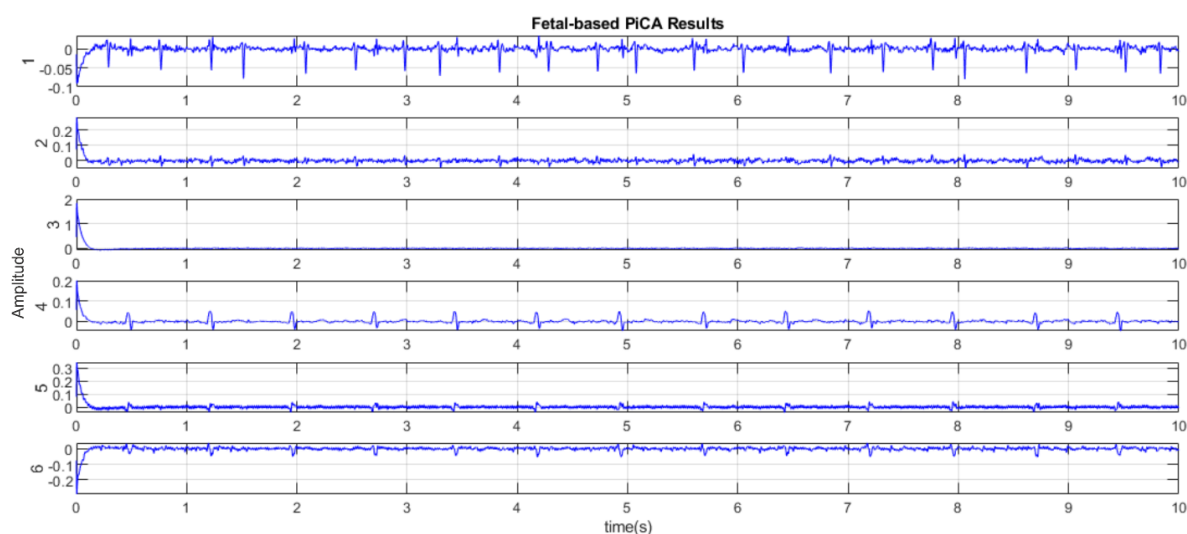

Figure 11. Extracted *f*ECG for ARR_01.

Same as previous, the R-peaks of the independent fetal component (2) are used to calculate the fetal ECG period for NR_02. The first component in resulting periodic components for NR_02 has the most remarkable similarity to the fetal ECG.
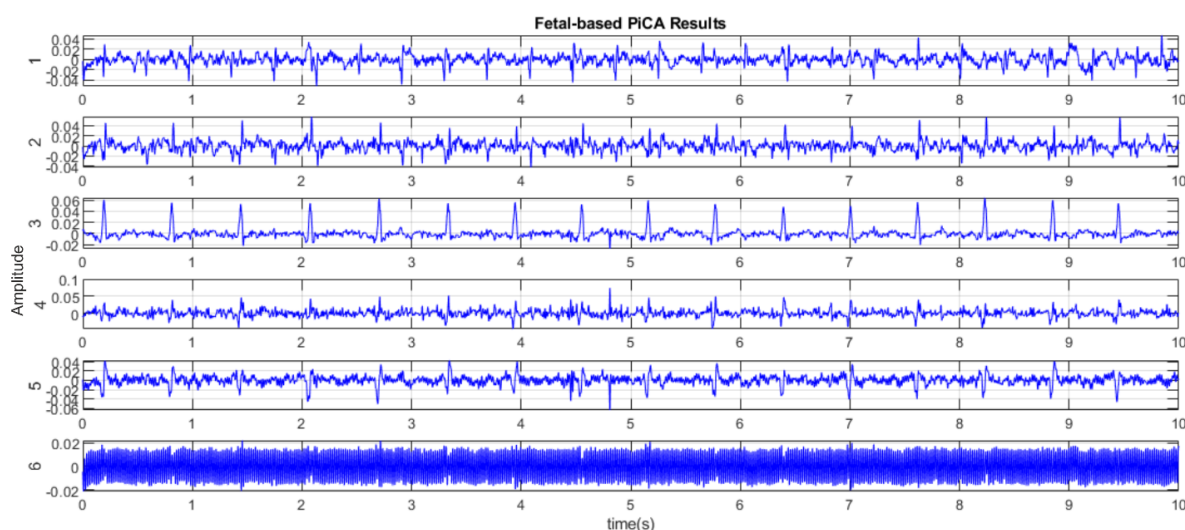

Figure 12. Extracted *f*ECG for NR_02.

Finally, R-peaks were detected in the *f*ECGs; the result for ARR_01 and NR_02 is shown in Figures 13 and 14. The top row of each figure depicts *f*ECG with marked R-peaks, and the bottom row shows the time between two sequential R-peaks (RR intervals).
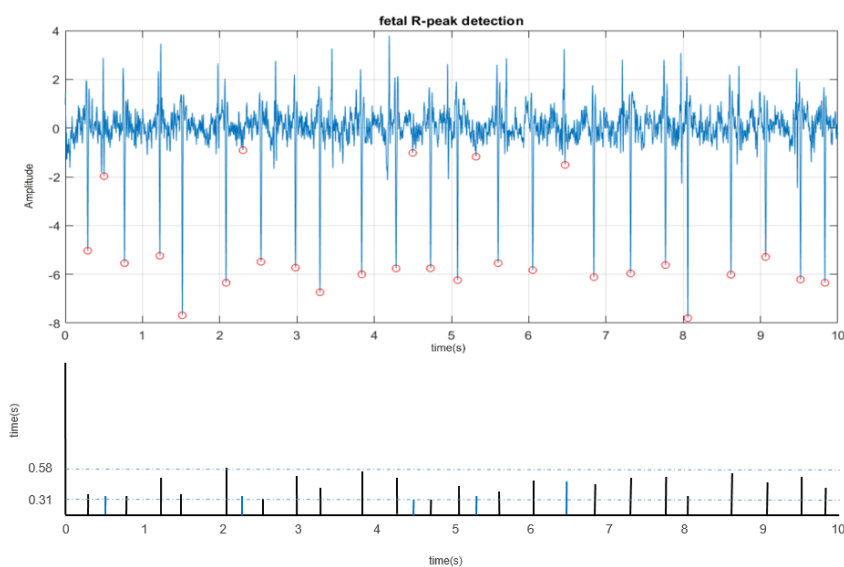
Figure 13. Detected *f*ECG R-peaks of ARR_01.

Figure 14. Detected *f*ECG R-peaks of NR_02.

The *f*ECG looks still noisy though R peaks are clearly demarcated, and P wave can be traced. Compared to NR_02, the R peaks in ARR_01 (bottom line) appear at irregular time intervals, and visually the P wave is unseen. However, the signs of irregularity occur between 6 and 7.5 seconds in NR_02. It can be considered as model perturbation and needs further investigation. Prolonged skewness and asymmetry of the RR-intervals can be used as a sign of arrhythmia or fetal heart failure and can potentially be used as a statistical indicator of the autonomic response to fetal hypoxia.

In practice, only up to 30% of abdominal ECG recordings allow the R-wave of the fetus to be clearly seen. When the fetus is in a cephalic presentation, the R waves on the ECG of the mother and

the fetus are in different planes (have opposite signs), so the fetal signals can be identified relatively easily. In the case of co-directional R-waves in the mother and fetus, the fetal signals can be identified by averaging them after the maternal signal has been removed. In some cases, the averaging every 4 beats enable to obtain a smooth shape of the beats [52].

5. Discussion

For evaluation resulting *f*ECG and its morphological elements, such as QRS-complex, P-wave, T-wave two statistical estimators, the Mean Squared Error (MSE) between raw and extracted ECG channels, and signal-to-noise ratio (SNR) between an original signal and the extracted component were used. The sensitivity of the selected components has been assessed.

MSE is the most widely used and also the simplest complete reference metric, which is calculated by squaring the differences between raw and extracted *f*ECG signal components and averaging them with the SNR of the related quantity. We used this statistic to assess the accuracy of the algorithm in terms of evaluating the *f*HR from their R-peaks. MSE is defined as [53].

$$MSE_{E1^k/E4^k} = \frac{1}{12} \sum_{i=1}^{12} \Delta h_i^2. \tag{8}$$

MSE metric was used to estimate the differences between matched values and computed *f*HR at twelve samples per one-minute segment, with, where denotes the assessed test *f*HR value on *i*-th segment and that denotes the referent *f*HR value for the same segment.

Finally, the SNR variation in decibels (*d*B) was calculated to find the relationship between the desired *f*HR signal and extracted component [54].

$$SNR = 20 \cdot log\left(\sqrt{\sum_{i=1}^{K} r_i^2 \Big/ \sum_{i=1}^{K} (f_i - r_i)^2}\right), \tag{9}$$

here *r* denotes a reference signal, and *f* is an extracted signal with *K* components.

The normalized MSE for ARR_01 and NR_02 between raw and extracted ECG channels are shown in Figure 15.
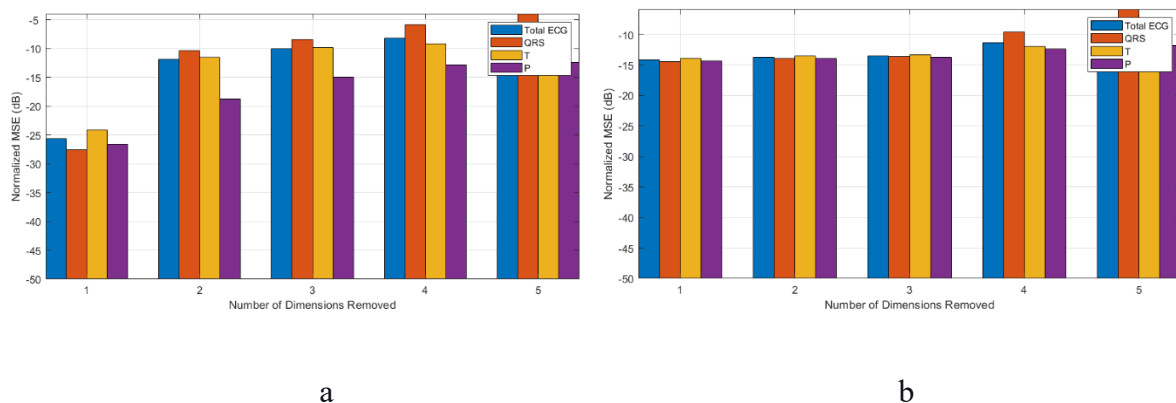

a
b

Figure 15. MSE on ARR_01 (a) and NR_02 (b).

The MSE in dB for the overall assessment of the isolated 5-lead *f*ECG signal for ARR_01 and NR_02 records is presented in Table 1. As can be seen, the MSE is different for the two records with the same preprocessing and analyzing procedure. All MSE for NR_02 is higher than MSE for ARR_01. This could be explained by the higher noise level of the original recording NR_02. MSE enables to track the clean-up quality of the original recording for the highlighted fetal ECG. The result obtained indicates a significant improvement in the recording after the preprocessing and analysis of the ECG recordings.

Table 1. Results of MSE averaging with the SNR of the related quantity for ARR_01 and NR_02 records.

Record	Channel 1	Channel 2	Channel 3	Channel 4	Channel 5
ARR_01	24,39	38,12	40,03	41,8	43,27
NR_02	35,85	36,28	36,5	38,67	40,69

The SNR estimates for the extracted fetal ECG, QRS-complex, P-wave, T-wave are shown in Figure 16, where the x-axis describes the noise level, and the y-axis describes the ECG channels.
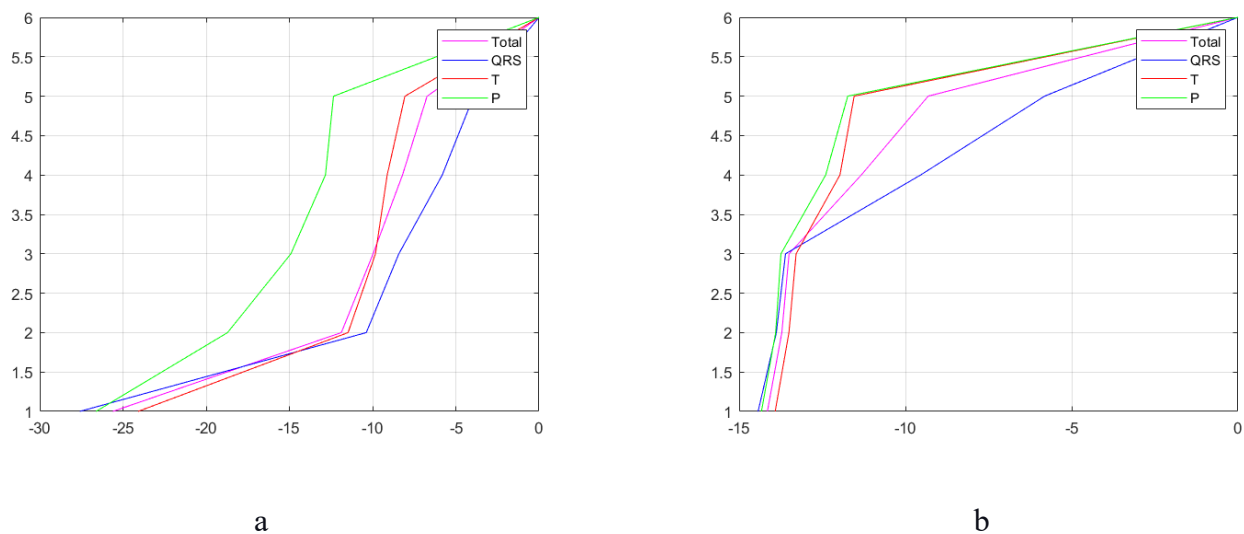

a   b

Figure 16. SNR on ARR_01 (a) and NR_02 (b).

The visualization of the results indicates that the SNR level for extracted *f*ECG varies for different morphological elements and channels. For instance, SNR for both records is the lowest for P-wave. This suggests that P-wave is the noisiest *f*ECG element and, therefore, be the biggest challenge for extraction. The QRS-complex is less noisy and, therefore, the most easily extracted component. As a general matter, human eyes unable to recognize fetal heart sounds when the SNR is lower than -15 dB. Our experiment shows a moderate SNR for the extracted *f*ECG that makes it possible recognition procedure. We compared our results with a set of similar studies conducted using both synthetic and real data from PhysioNet (see Table 2). In most baseline research, two real ECG datasets (adfecgdb and DAISY) and synthesized (FECGSYNDB) ECG datasets were used.

Table 2. SNR results for multichannel *f*ECG extracted from abdominal mixture.

Paper	Methods	SNR(dB)
Sargolzaei et al., 2008 [55]	adaptive filter, SVD, ICA, wavelets	-19.786 to -12.24
Tang et al., 2016 [56]	repetition frequency of heart sounds	-26.7 to -4.4
Fotiadou et al, 2018 [57]	time sequenced adaptive filter	-15 to -12
Taha et al., 2020 [58]	input-mode and output-mode adaptive filters with BSS	-30 to 0
Ours QRS	second-order zero-phase lowpass filter,	-27.59 to -3.926
Ours T-wave	PCA, JADE, GEVD, periodic component	-24.09 to -8.06
Ours P-wave	analysis	-26.62 to -11.74

Results obtained in this study are comparable to the benchmarks, but as shown above, the mixing technique allows the detection of arrhythmias and ectopic contractions when sudden, and short-term changes in the morphology of the *f*ECG signal occur. It can adapt quickly to abrupt changes in *f*ECG, enabling the identification of new artefacts. Moreover, since the target application of this technology is improving the quality of the fetal ECG to detect hypoxia, it is possible to propose the inclusion of the results in the risk assessment scheme for further investigation on a long-term basis.

In summary, non-invasive *f*ECG has the potential to monitor fetal heart rate and *f*ECG morphological parameters. In terms of fetal hypoxia, this information could be included in the auto-generated screening tool to achieve early warning on fetus' safety, identifying fetuses at risk of hypoxia, and enabling early intervention to improve perinatal outcomes. In this respect, the following should be taken into account: 1) separate abnormalities detected in fetal heart rate in the absence of disturbances of beat-to-beat variability or decelerations may not flag fetal hypoxia; 2) the likelihood of fetal hypoxia increases when there are signs of baseline bradycardia coupled with the loss of beat-to-beat variability and decelerations [52].

Following up on our previous research, the updated profile of pregnancy complications associated with fetal hypoxia [12] includes a new section based mostly on *f*ECG data received on non-invasive techniques. As is the case of the fetal biophysical profile that combines data obtained from different sources and calculates the score points, the profile assigns different scores for abnormal and normal points to achieve the risk level. Table 3 shows the profile of pregnant mother on both the fetal and maternal status related to the presence or absence of pregnancy complications associated with intrauterine hypoxia.

Table 3. The profile of fetal and maternal status associated with intrauterine hypoxia.

Parameters	Abnormal	Normal
Maternal age, years [59,60,61*]	< 20, $> 35^*$	20 to 35
Combination of maternal height (cm) and Body Mass Index (BMI), (kg/m^2) [62]	< 156 and BMI > 25	≥ 156, BMI < 25
Adjusted gestational weight gain, kg [63]	> 13.6	< 13.6
General Gynaecological issues [58]	yes	no
Urinary tract infection during pregnancy [61]	yes	no
Blood pressure before pregnancy [60]	$> 130/85$	$< 130/85$

Continued on next page

Parameters	Abnormal	Normal
Maternal smoking [59]	yes	no
Rh sensitization [59,63]	yes	no
Illicit drug use [63]	yes	no
Antidepressant use [63]	yes	no
The number of fetuses in a pregnancy [59,60]	> 1	1
Previous fetal death/stillbirth [63]	yes	no
Blood pH [58]	< 7.2	≥ 7.2
Chronic somatic pathologies [58,59]	yes	no
Preeclampsia (new-onset hypertension after 20 weeks gestation with new-onset proteinuria) [64]	yes	no
Intrauterine infections [59]	yes	no
Placental abruption [59,63]	premature	timely
Erythrocyte Sedimentation Rate, ESR (21 weeks gestation) (mm/h) [12]	26–69	25
ESR (30 weeks) (mm/h) [12,65]	4–69	30–35
Ultrasound grading of placental maturity (the degree of the placental maturity) 30–38 weeks gestation (grade) [12,65]	I	I-II
Vertical size of amniotic fluid on ultrasound 30–38 weeks gestation (mm) [12,59]	269–306	82–268
Vertical size of amniotic fluid on ultrasound 20–24 weeks gestation (mm) [12,59]	> 200	< 200
Skewness of fetal RR intervals [30]	yes	no
Loss of fetus beat-to-beat variability coupled with variable or late decelerations [52]	yes	no
ƒHR (± 2 standard deviations), bpm [52,66*]	< 120 (< 110)*, >160 (> 150)*	120 to 160 110* to 150*
Short term ƒHR variation (no longer than 60 min) [66]	10 to 15 bpm	
PR vs ƒHR [46,52]	inverted relationship	direct correlation
Ratio between the amplitude of the fetal QRS complex and that of the T wave [46]	≥ 0.25	< 0.25
Hypoxia index (HI) (during labor) [47]	*Hi* $\leq$ 24	*Hi* > 25

6. Conclusions

In this study, the approach for automatic ƒECG processing and updating profile for fetal hypoxia risk estimation was proposed. The ultimate goal was to investigate the possibilities of extraction a ƒECG from signal recorded non-invasively on the mother's abdomen and assess the feasibility of the ƒECG morphological evaluation to be included in the automatic screening tool for identifying fetuses at high risk of hypoxia. The set of new artefacts were defined and included in the profile of the pregnant mother for detecting hypoxic fetus. This is the first step towards a comprehensive risk score for fetal hypoxia that can be used not only in a clinical setting but also for remote outpatient monitoring

enabling pregnant women to receive timely prenatal and antenatal care, which is crucial in high-risk pregnancies. The main advantage of including ƒECG parameters into the risk profile is its simplicity of use and programming. As compared to others, this approach can be used for measuring the risk of fetal hypoxia in-utero. Particular attention was paid to ƒECG signal extraction from maternal abdominal ECG signals using a hybrid filtering technique. The blind source separation, the GEVD and periodic component analysis were applied at the stage of fetal ECG extraction. Detected R-peaks were used to determine RR-intervals and average ƒHR per minute. The study showed that the quality of ƒECG extraction is highly dependent on extraneous noise; under equal processing and signal extraction conditions, the MSE and SNR results are slightly different for ARR_01 and NR_02 records. For all that, the result of MSE and SNR shows that our approach is suitable for fetal heartbeat extraction and further ƒHR analysis from multiple abdominal recording. Moving forward, the appropriate choice of filters could significantly improve the quality and adequacy of extracted ƒECG signals and raise the prospect of their clinical approval. Therefore, the next work will be aimed at fine-tuning and studying different filtering methods for more accurate ƒECG extraction and fetal R-peaks detection. In this aspect, further work will focus on performing automatic extraction of morphological features such as PR intervals, QT intervals and ST segments. Non-linear control stability of heartbeat based on modified Zeeman's heartbeat models [67] will also be discovered. Elaboration and validation of technology for ƒHRV and fetal risk assessment through the hypoxia index are also the subjects of future research, as well as an integrated model for fetal hypoxia risk assessment. We also expect that this approach will enable the provision of new medical services with improved accuracy and the advantages of low cost and easy implementation in the near future.

7.   Limitations

We pay attention to the following limitations of this study. First, given the small number of published datasets, there was not enough data for analysis. Second, signal filters reduce noise and improve the signal, but at the same time, they can cause phase delays that affect morphology and temporal alignment between different leads. Next, there is a piece of evidence [68] that computerized interpretation of CTG in women with continuous fetal monitoring in labor did not improve clinical outcomes. Finally, this technique has not been tested for real data with the pregnant mother, which raises some doubts about the quick win of non-invasive ƒECG as an additional method for diagnosing fetal hypoxia. Multifetal pregnancy has not been taken into consideration during signal processing but is included in the profile. Clinical validation and more deep analysis are needed to completely adapt and include these parameters into the risk assessment tool.

Conflict of interest

The authors declare that the research was conducted in the absence of any commercial or financial relationships that could be construed as a potential conflict of interest.

References

1. C. Gravett, L. O. Eckert, M. G. Gravett, D. J. Dudley, E. M. Stringer, T. B. M. Mujobu, et al., Non-reassuring fetal status: case definition & guidelines for data collection, analysis, and presentation of immunization safety data, *Vaccine*, **34** (2016), 6084.

2. J. Fahey, T. L. King, Intrauterine asphyxia: clinical implications for providers of intrapartum care, *J. Midw. Womens Health*, **50** (2005), 498–506.

3. R. K. Freeman, T. J. Garite, M. P. Nageotte, L. A. Miller, *Fetal Heart Rate Monitoring*, 4th edition, Philadelphia, Lippincott Williams and Wilkins, 2012.

4. *GE Healthcare*, Novii Wireless Patch System, Available from: https://www.gehealthcare.com/products/maternal-infant-care/fetal-monitors/novii-wireless-patch-system.

5. M. Mhajna, N. Schwartz, L. Levit-Rosen, S. Warsof, M. Lipschuetz, M. Jakobs, et al., Wireless, remote solution for home fetal and maternal heart rate monitoring, *Am. J. Obstet. Gynecol. MFM*, **2** (2020), 100101.

6. R. Tapia-Conyer, S. Lyford, R. Saucedo, M. Casale, H. Gallardo, K. Becerra, et al., Improving perinatal care in the rural regions worldwide by wireless enabled antepartum fetal monitoring: a demonstration project, *Int. J. Telemed. Appl.*, 2015.

7. E. M. Graatsma, B. C. Jacod, L. A. J. V. Egmond, E. J. H. Mulder, G. H. A. Visser, Fetal electrocardiography: feasibility of long-term fetal heart rate recordings, *Bjog*, **116** (2009), 334–338.

8. R. Martinek, R. Kahankova, B. Martin, J. Nedoma, M. Fajkus, A novel modular fetal ECG STAN and HRV analysis: towards robust hypoxia detection, *J. Health Care Technol.*, **27** (2019), 257–287.

9. J. Balayla, G. Shrem, Use of artificial intelligence (AI) in the interpretation of intrapartum fetal heart rate (FHR) tracings: a systematic review and meta-analysis, *Arch Gynecol. Obstet.*, **300** (2019), 7–14.

10. G. M. Ungureanu, J. W. M. Bergmans, S. G. Oei, A. Ungureanu, W. Wolf, The event synchronous canceller algorithm removes maternal ECG from abdominal signals without affecting the fetal ECG, *Comput. Biol. Med.*, **39** (2009), 562–567.

11. A. Agostinelli, S. Fioretti, F. D. Nardo, L. Burattini, Clinical application of the segmented-beat modulation method for fetal ECG extraction, in *Proceedings of the 12th International Workshop on Intelligent Solutions in Embedded Systems (WISES)*, Ancona, IEEE Press, (2015), 35–40.

12. I. Skarga-Bandurova, T. Biloborodova, M. Nesterov, Extracting interesting rules from gestation course data for early diagnosis of neonatal hypoxia, *J. Med. Syst.*, **43** (2019), 1–10.

13. R. Sameni, G. D. Clifford, A review of fetal ECG signal processing; issues and promising directions, *Open Pacing, Electrophysiol. Ther. J.*, **3** (2010), 4–20.

14. D. Taralunga, M. G. Ungureanu, I. Gussi, R. Strungaru, W. Wolf, Fetal ECG extraction from abdominal signals: a review on suppression of fundamental power line interference component and its harmonics, *Comput. Math. Method. Med.*, (2014), 239060.

15. J. Jezewski, A. Matonia, T. Kupka, D. Roj, R. Czabanski, Determination of the fetal heart rate from abdominal signals: evaluation of beat-to-beat accuracy in relation to the direct fetal electrocardiogram, *Biomed. Eng.*, **57** (2012), 383–394.

16. J. Behar, A. Johnson, G. D. Clifford, J. Oster, A comparison of single channel fetal ECG extraction methods, *Ann. Biomed. Eng.*, **42** (2014), 1340–1353.

17. D. Jagannath, A. I. Selvakumar, Issues and research on foetal electrocardiogram signal elicitation, *Biomed. Signal Process. Control*, **10** (2014), 224–244.

18. S. Ravindrakumar, K. B. Raja, Fetal ECG extraction and enhancement in prenatal monitoring—Review and implementation issues, in *Proceedings of the IEEE Trendz in Information Sciences &Computing (TISC)*, Chennai, India, (2010), 16–20.

19. N. Widatalla, Y. Kasahara, Y. Kimura, A. Khandoker, Model based estimation of QT intervals in non-invasive fetal ECG signals, *Plos one*, **15** (2020), e0232769.

20. Q. Yu, H. Yan, L. Song, W. Guo, H. Liu, J. Si, et al., Automatic identifying of maternal ECG source when applying ICA in fetal ECG extraction, *Biocybern. Biomed. Eng.*, **38** (2018), 448–455.

21. S. Padhy, *Mult acne monitoring bioimpedance deviceilead ECG data analysis using SVD and higher-order SVD*, Doctoral dissertation, Ph. D. thesis, Indian Institute of Technology Guwahati, India, 2017.

22. A. D. Deogire, Multi lead fetal QRS detection with principal component analysis, in *IEEE 2018 3rd International Conference for Convergence in Technology (I2CT)*, (2018), 1–5.

23. I. Perova, Y. Bodyanskiy, Adaptive human machine interaction approach for feature selection-extraction task in medical data mining, *IJC* **17** (2018), 113-119.

24. M. Fatemi, R. Sameni, An online subspace denoising algorithm for maternal ECG removal from fetal ECG signals, *IJST-T Electr. Eng.*, **41** (2017), 65–79.

25. Z. L. Zhang, Y. Ye, Extended Barros's extraction algorithm with its application in fetal ECG extraction, in *2005 International Conference on Neural Networks and Brain*, Beijing, (2005), 1077–1080.

26. S. Redif, Fetal electrocardiogram estimation using polynomial eigenvalue decomposition, *Turk. J. Electr. Eng. Comput. Sci.*, **24** (2016), 2483–2497.

27. G. H. Golub, C. F. van Loan, *Matrix Computations*, 3nd edition, Baltimore, The Johns Hopkins University Press, 1996.

28. M. Suganthy, Analysis of R-peaks in fetal electrocardiogram to detect heart disorder using fuzzy clustering, in *IEEE 5th International Conference for Convergence in Technology (I2CT)*, (2019), 1–4.

29. N. E. Huang, Z. Wu, S. R. Long, Hilbert-Huang transform, *Scholarpedia J.*, **3** (2008), 2544.

30. R. Jaros, R. Martinek, R. Kahankova, Non-adaptive methods for fetal ECG signal processing: a review and appraisal, *Sensors*, **18** (2018), 3648.

31. A. Hyvarinen, Fast and robust fixed-point algorithms for independent component analysis, *IEEE Trans. Neural Netw.*, **10** (1999), 626–634.

32. J. F. Cardoso, Source separation using higher order moments, in *Proceedings of the IEEE International Conference on Accoustics, Speech and Signal Processing*, (1989), 2109–2112.

33. L. Yuan, Y. Yuan, Z. Zhou, Y. Bai, S. Wu, A fetal ECG monitoring system based on the Android smartphone, *Sensors*, **19** (2019), 446.

34. J. G. Aida, N. Castaneda-Villa, Blind extraction extraction of fetal and maternal components from the abdominal electrocardiogram: An ICA implementation for low-dimensional recordings, *Biomed. Signal Process. Control*, **58** (2020), 101836.

35. I. Romero, PCA-based noise reduction in ambulatory ECGs, in *Proceedings of the IEEE Computing in Cardiology*, Belfast, UK, (2010), 677–680.

36. G. Liu, Y. Luan, An adaptive integrated algorithm for noninvasive fetal ECG separation and noise reduction based on ICA-EEMD-WS, *Med. Biol. Eng. Comput.*, **53** (2015), 1113–1127.

37. A. Gupta, M. Srivastava, V. Khandelwal, A. Gupta, A novel approach to fetal ECG extraction and enhancement using blind source separation (BSS-ICA) and adaptive fetal ECG enhancer (AFE), in *Proceedings of the IEEE 6th International Conference on Information, Communications & Signal Processing*, Singapore, (2007), 1–4.

38. M. Kotas, Combined application of independent component analysis and projective filtering to fetal ECG extraction, *Biocybern. Biomed. Eng.*, **28** (2008), 75–93.

39. R. Sameni, *Extraction of Fetal Cardiac Signals from an Array of Maternal Abdominal Recordings. Signal and Image processing*, Institut National Polytechnique de Grenoble-INPG, Sharif University of Technology (SUT), 2008.

40. J. F. Cardoso, A. Souloumiac, Blind beamforming for non-gaussian signals, in *IEEE proceedings F (radar and signal processing)*, **140** (1993), 362–370.

41. F. Jamshidian-Tehrani, R. Sameni, Fetal ECG extraction from time-varying and low-rank noninvasive maternal abdominal recordings, *Physiol. Meas.*, **39** (2018), 125008.

42. R. Sameni, C. Jutten, M. B. Shamsollahi, Multichannel electrocardiogram decomposition using periodic component analysis, *IEEE Trans. Biomed. Eng.*, **55** (2008), 1935–1940.

43. J. Jezewski, D. Roj, J. Wrobel, K. Horoba, A novel technique for fetal heart rate estimation from Doppler ultrasound signal, *Biomed. Eng. Online*, **10** (2011), 92.

44. M. Malik, Heart rate variability: standards of measurement, physiological interpretation and clinical use. Task Force of the European Society of Cardiology and the North American Society of Pacing and Electrophysiology, *Circulation*, **93** (1996), 1043–1065.

45. G. Magenes, M. G. Signorini, D. Arduini, Classification of cardiotocographic records by neural networks, in *Proceedings of the IEEE-INNS-ENNS International Joint Conference on Neural Networks. IJCNN 2000. Neural Computing: New Challenges and Perspectives for the New Millennium*, **3** (2000), 637–641.

46. I. Amer-Wahlin, P. Bördahl, T. Eikeland, C. Hellsten, H. Norén, T. Sörnes, et al., ST analysis of the fetal electrocardiogram during labor: Nordic observational multicenter study, *J. Matern. Fetal Neonatal Med.*, **12** (2002), 260–266.

47. K. Maeda, M. Utsu, Rise & fall of fetal heart rate, the principle of fetal monitoring: hypoxia index prevents cerebral palsy, *J. Gynecol. Res. Obstet.*, **4** (2018), 036–038.

48. K. Maeda, Improved outcome with novel studies in fetal monitoring, *Sci. J. Gynecol. Obstet.*, **2** (2019), 001-004.

49. R Sameni, The open-source electrophysiological toolbox (OSET), version 3.14, 2018. Available from: http://www.oset.ir.

50. J. A. Behar, L. Bonnemains, V. Shulgin, J. Oster, O. Ostras, I. Lakhno, Noninvasive fetal electrocardiography for the detection of fetal arrhythmias, *Prenat. Diagn.*, **39** (2019), 178–187.

51. A. L. Goldberger, L. A. N. Amaral, L. Glass, J. M. Hausdorff, P. Ch. Ivanov, R. G. Mark, et al., PhysioBank, PhysioToolkit, and PhysioNet: Components of a new research resource for complex physiologic signals, *Circulation*, **101** (2000), e215–e220.

52. J. J. Volpe, *Neurology of the Newborn*, 5nd edition, Philadelphia, PA, Saunders/Elsevier, (2008), 1094.

53. I. Silva, J. Behar, R. Sameni, T. Zhu, J. Oster, G. D. Clifford, et al., Noninvasive fetal ECG: The physioNet/computing in cardiology challenge 2013, *Comput. Cardiol. 2013*, (2013), 149–152.

54. J. Behar, F. Andreotti, J. Oster, G. D. Clifford, A bayesian filtering framework for accurate extracting of the non-invasive FECG morphology, in *Processing of the Computing in Cardiology Conference (CinC)*, **41** (2013), 53–60.

55. S. Sargolzaei, K. Faez, A. Sargolzaei, Signal processing based for fetal electrocardiogram extraction, in *2008 International Conference on BioMedical Engineering and Informatics*, **2** (2008), 492–496.

56. E. Fotiadou, J. O. E. H. van Laar, S. G. Oei, Enhancement of low-quality fetal electrocardiogram based on time-sequenced adaptive filtering, *Med. Biol. Eng. Comput.*, **56** (2018), 2313–2323.

57. L. Y. Taha, E. Abdel-Raheem, Fetal ECG extraction using input-mode and output-mode adaptive filters with blind source separation, *Can. J. Elect. Comput. E.*, **43** (2020), 295–304.

58. O. V. Mertsalova, *Perinatal hypoxic lesions of the central nervous system of the fetus in high-risk pregnant women (diagnosis, prognosis, optimization of pregnancy and childbirth)*, dis Dr. of Medical Sciences, Kharkiv, 2002.

59. M. Martinez-Biarge, J. Diez-Sebastian, C. J. Wusthoff, E. Mercuri, F. M. Cowan, Antepartum and intrapartum factors preceding neonatal hypoxic-ischemic encephalopathy, *Pediatrics*, **132** (2013), 952–959.

60. I. Milsom, L. Ladfords, K. Thiringer, A. Niklasson, A. Odeback, E. Thornberg, Influence of maternal, obstetric and fetal risk factors on the prevalence of birth asphyxia at term in a Swedish urban population, *Acta Obstet. Gynecol. Scand.*, **81** (2002), 909–917.

61. S. J. Parker, M. Kuzniewicz, H. Niki, Y. W. Wu, Antenatal and intrapartum risk factors for hypoxic-ischemic encephalopathy in a US birth cohort, *J. Pediatr.*, **203**, (2018), 163–169.

62. L. Liljestrom, A. K. Wikstrom, J. Agren, M. Jonsson, Antepartum risk factors for moderate to severe neonatal hypoxic ischemic encephalopathy: a Swedish national cohort study, *Acta Obstet. Gynecol. Scand.*, **97** (2018), 615–623.

63. P. J. Peebles, T. M. Duello, J. C. Eickhoff, R. M. McAdams, Antenatal and intrapartum risk factors for neonatal hypoxic ischemic encephalopathy, *J. Perinatol.*, **40**, (2020), 63–69.

64. L. Thompson, S. Crimmins, B. Telugu, S. Turan, Intrauterine hypoxia: clinical consequences and therapeutic perspectives, *Res. Rep. Neonatol.*, **5** (2015), 79–89.

65. T. Biloborodova, I. Skarga-Bandurova, Medical Data Analysis and Modelling, Book 1: Processing Medical Records for Predictive Analytics, Kyiv, 2021.

66. S. Vannuccini, C. Bocchi, F. M. Severi, F. Petraglia, Diagnosis of fetal distress, *Neonatology*, (2018), 105–127.

67. M. Abdelhady, Y. Kondratenko, W. Abouelwafa, D. Simon, Stability analysis of heartbeat control based on the zeeman framework, in *Processing of 10th IEEE International Conference on Intelligent Data Acquisition and Advanced Computing Systems: Technology and Applications, IDAACS 2019*, **2** (2019), 824–829.

68. INFANT Collaborative Group, Computerised interpretation of fetal heart rate during labour (INFANT): a randomised controlled trial, *Lancet*, **389** (2017), 1719–1729.